Elucidation of the IR of Cu and Mn substituted intraframework SiBEA zeolites

Etienne Hessou, Michael Badawi, Laetitia Valentin, Guy Atohoun, Stanislaw Dzwigaj, Monica Calatayud, Frederik Tielens

Elucidation of the IR of Cu and Mn substituted intraframework SiBEA zeolites

Etienne P. Hessou[a,b], Michael Badawi[c], Laetitia Valentin[d], Guy Atohoun[b], Stanislaw Dzwigaj[d]

Monica Calatayud[e] and Frederik Tielens[a,*]

[a] General Chemistry (ALGC) – Materials Modelling Group, Vrije Universiteit Brussel (Free University Brussels-VUB), Pleinlaan 2, 1050 Brussel, Belgium.

[b] Laboratoire de Chimie Théorique et de Spectroscopie Moléculaire LACTHESMO, Université d'Abomey-Calavi, Bénin.

[c] Laboratoire de Physique et Chimie Théoriques LPCT – UMR CNRS 7019, Université de Lorraine, Vandœuvre-lès-Nancy, France.

[d] Laboratoire de Réactivité de Surface, Sorbonne Université-CNRS, UMR 7197, 4 Place Jussieu, Case 178, F-75252 Paris, France

[e] Laboratoire de Chimie Théorique, Sorbonne Université-CNRS, UMR 7616, 4 Place Jussieu, Case 137, F-75252 Paris, France

*author to whom correspondence should be sent: frederik.tielens@vub.be

Abstract

Copper and manganese modified zeolites play key roles in selective oxidation catalytic reactions. Combining Density Functional Perturbation Theory (DFPT) implemented in VASP, and infrared spectroscopy experiments, we have studied and elucidated the incorporation of Cu^{2+} and Mn^{2+} in the framework of SiBEA zeolite. Six isomers are investigated for both models CuSiBEA and MnSiBEA. The energy stability study identified the most stable isomer in each case, which correspond to M-O2 bent moieties in the vicinity of hydroxyl groups. The isomers are then characterized by experimental and theoretical IR spectra. Both experimental and calculated IR spectra are in good agreement highlighting the presence of active sites (Cu-OH and Mn-OH) in the obtained models. The accurate molecular description of the nature of the active sites presented in this work will be important for understanding the catalysis going on and for developing novel catalytic processes.

Keywords: DFT; IR; CuSiBEA; MnSiBEA; Zeolites

1. Introduction

Transition metal ionic centers play in important role in catalysis, and especially in heterogenous catalysis [1,2]. The incorporation of nano sized transition metals in oxides, and in silica based materials, has shown to enable the fine tuning and control of the specific reactivity of such materials [3–14].

For decades transition metal oxides have been studied in and on different solid materials, and particularly in zeolites [3,15–21]. The presence of these transition metal sites in the zeolites has shown to introduce both acid/base as well as redox properties in the catalysts, together with the intrinsic size selectivity associated to the open structure containing channels and cages.
The possibility to obtain extra and intra-framework transition metal sites makes zeolites extremely versatile heterogenous catalysts [22–24]. In order to understand their reactivity, in-depth characterization is needed, and the combination of experimental and theoretical methods provide highly valuable information on the atomic level [25–27].

Recently, an increased interest in copper- and manganese-containing zeolite catalysts aroused, due to the high efficiency in processes important for environment protection such as selective catalytic reduction of NO with ammonia [28–32] and oxidation of volatile organic compounds (VOC) [33–35]. The preparation of Cu- and Mn-containing zeolites is commonly achieved by conventional techniques of postsynthesis modification such as wet impregnation and ion-exchange or direct synthesis in hydrothermal conditions. However, copper and manganese in zeolites obtained by these conventional preparation procedures may be present at various oxidation states and chemical environments because these preparation methods do not allow controlling state of copper and manganese in the zeolite structure. As a result, Cu- and Mn containing zeolite materials with different kinds of copper and manganese species could be formed.

The presence of different types of active sites might lead to poor selectivity in many reactions, it is thus desirable to obtain a stable and high selective catalyst during the synthesis to hinder side reactions and to avoid fast deactivation. Thus, the optimization of current synthesis methods as well as the development of new methods of zeolite catalyst preparation are highly needed.

In this work we investigate and discuss Mn^{2+} and Cu^{2+} substitutions or insertions in the BEA zeolite framework, geometrically, energetically and spectroscopically (IR) in other to elucidate and localize active sites in these materials for applications in catalysis. The materials are synthesized and characterized by experimental IR techniques, combined with theoretical ab initio approaches, so as to determine both structure and stability around the metal sites.

Thus, materials are first characterized by periodic Density Functional Theory (DFT) to determine the energetics and to simulate the IR spectroscopic properties. A set of 6 possible metal intraframework

sites for Cu and Mn with neighboring hydroxyl groups is considered. The procedure is similar to previous studies where transition metal/Si substitution is investigated in simple sodalite (SOD) structure [3–5,36,37] and in BEA zeolite [3–8,37–39]. As a result, accurate information about the thermodynamic stability of the Cu- and Mn- sites is provided, together with in silico IR spectra that guide the comparison with experimental results.

In the experimental counterpart, the modified zeolites are synthesized using a two-step postsynthesis method, composed of dealumination and impregnation steps, developed earlier by Dzwigaj et al. [40–44] to obtain Cu and Mn containing SiBEA zeolite with isolated, mononuclear Cu and Mn species. The CuSiBEA and MnSiBEA prepared by this postsynthesis method contains Cu(II) and Mn(II) species incorporated into the intraframework positions. The incorporation of copper and manganese by two-step postsynthesis method as Cu(II) and Mn(II) species has been proved in our previous works by DR UV-vis, EPR, FTIR-CO, XPS, EXAFS and XANES investigations and published in [45,46]

The presence of Cu(II) species in $Cu_{2.0}$SiBEA sample has been earlier proved [45] by DR UV-vis, EPR and XPS spectra of $Cu_{2.0}$SiBEA sample. The DR UV-vis spectrum showed a broad band at 835 nm characteristic of d-d transitions and an intense charge-transfer (CT) band at 280 nm. These bands could be assigned to the d-d transition of Cu^{2+} ($3d^9$) and CT O^{2-} ^{a} Cu^{2+} transition of isolated mononuclear Cu(II) being in coordination with lattice oxygen, respectively [47–50]. The EPR spectrum of Cu2.0SiBEA showed at 298 K isotopic signal (g_{iso} = 2.19) typical of octahedral Cu(II) species [51–55]. Moreover, our earlier FTIR investigation [46] using CO as a probe molecule have confirmed that in Cu2.0SiBEA sample, prepared by two_step postsynthesis method, cobalt is present as isolated mononuclear copper(II) species. This is proved by intense band at 2202 cm^{-1} atributted to Cu(II)-CO adducts.

The presence of Cu(II) species in CuSiBEA samples has been confirmed in our earlier investigation using XPS studies [56]. Because Cu 2p3/2 core excitation considered alone does not allow determining the oxidation state and coordination of copper without doubt, the CuSiBEA samples are characterized by using both X-ray excited Cu 2p3/2 and Cu L3VV transitions. Therefore, a shake-up satellites associated with Cu 2p3/2 peak and a modified Auger parameter were employed for Cu oxidation state determination. In addition, the shake-up satellite associated with Cu 2p3/2 peak appearing at about 945 eV for CuSiBEA, confirms that copper is mainly present in (II) oxidation state. The low intensity of the satellite for all CuSiBEA is probably due to high copper dispersion in the zeolite structure as isolated tetracoordinated Cu(II) [57]. The presence of second component (B) for Cu 2p3/2 and Cu 2p1/2 at higher BE of about 936–937 eV and 956–957 eV, respectively, reveals that probably some amount of octacoordinated Cu(II) species is also present, which is in line with similar studies on Cu/Y zeolite reported by Narayana et al. [58].

The presence of Cu(II) species in CuSiBEA, prepared by two-step postsynthesis method has been evidenced by the Fourier transform of k3 -weighted Cu K-edge EXAFS and XANES spectra [45]. The Fourier transform of CuSiBEA shows only one single and intense peak at 1.6–1.7 A˚ due to the presence in the first shell of Cu(II) of four oxygen neighbours [59]. For CuSiBEA, a small pre-edge peak at 8975 eV is observed in XANES spectrum due to the 1s --> 3d transition characteristic of Cu^{2+} [60].

In conclusion, the combined DR UV–vis-NIR, EPR, FTIR-CO, XPS, EXAFS and XANES investigations suggest that copper in CuSiBEA zeolite is mainly present as isolated mononuclear Cu(II) species.

The presence of Mn(II) species in MnSiBEA sample has been earlier evidenced by XPS with the binding energy of $Mn2p_{3/2}$ in the range of 640.6 and 642.0 eV [61] and by XANES spectroscopy [62].

The samples are then characterized by IR spectroscopy.

2. Computational details

The theoretical calculations have been performed using the Vienna Ab Initio Simulation Package (VASP) [63]. Density functional theory was used applying the augmented plane wave method (PAW) [64] to describe the electron-ion interactions with a cut-off energy of 500 eV [6,65]. The Perdew Burke Ernzerhof functional (PBE) [66] was employed, and the Kohn–Sham spin-polarized equations were solved self-consistently until the energy difference of the cycles is smaller than 10^{-6} eV. The atomic positions were fully optimized until all forces were smaller than 0.01 eV/Å per atom. All computations were performed only at the Γ-point due to the large size of the unit cell.

To accurately describe the zeolite structure, van der Waals (vdW) interactions should be included [67–70]. In this work, the Grimme D3-correction method by introducing the Becke-Johnson damping potential [71,72] was used to compute the substitution energy of each M-substituted BEA zeolite, as described below.

To simulate the vibrational frequencies and intensities of IR spectra, the Density Functional Perturbation Theory (DFPT) [73–76] was employed on our relaxed structures. In the dipolar approximation, the intensity of i_{th} normal mode of vibration at a frequency ω_i, is proportional to the square of the change of dipole moment associated with the atomic motion along the eigenvector e_i of that mode:

$$I_i \propto \left|\frac{\partial P}{\partial R} ei\right|^2 = \sum_\alpha \left[\sum_l \sum_\beta Z^*_{\alpha\beta}(l) e_{i,\beta}(l)\right]^2$$

Where, $e_{i,\beta}(l)$ is the displacement of i_{th}-atom in the eigenvector of the i_{th} normal mode and $Z^*_{\alpha\beta}(l) = \frac{\partial P\alpha}{\partial R\beta(l)}$ is the Born charge of the i_{th} atom, as implemented in VASP [77].

To build the MBEA zeolite model, the whole orthorhombic unit cell with dimensions (12.6 Å × 12.6 Å × 26.2 Å) of siliceous BEA is used (Figure 1) [6,78]. According to crystallographic data, zeolite BEA contains nine different tetrahedral-sites (T-sites) [6,79]. There are basically 192 atoms in the unit cell with 64 Si atoms and 128 O atoms. It is known that BEA has 9 distinct crystallographic T-sites. It was chosen to substitute one T site on position 1 because this position has been identified as most stable for incorporation of some metals [6,78]. The substitution of Si^{4+} by M^{2+} leads to a structure with 194 atoms, including $2H^+$ ions to keep electroneutrality. The final substituted T-site contains an M ion surrounded by two Si-OH groups and anchored via 2 Si-O-M linkages, as can be seen in Figure 2 and Figure 4.

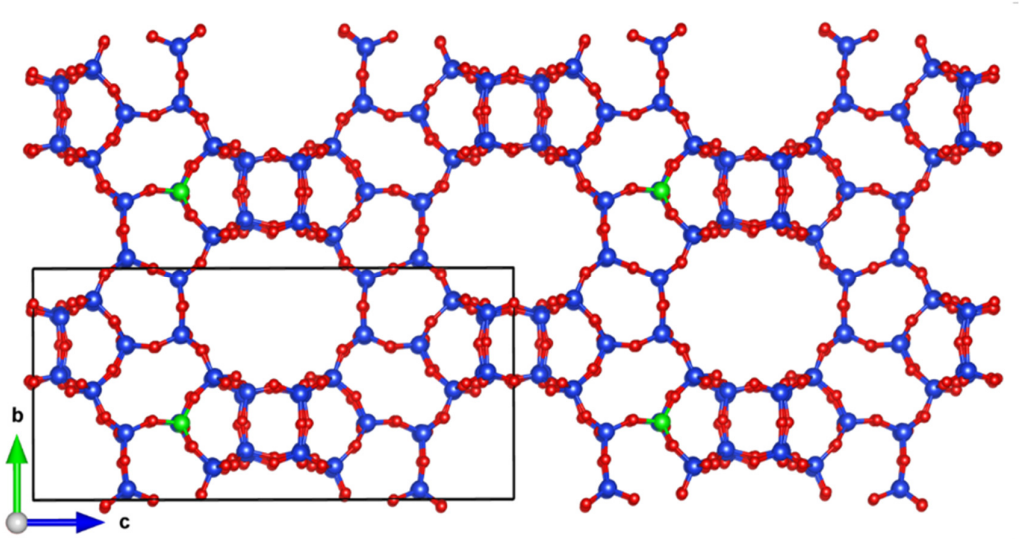

Figure 1. BEA zeolite unit cell used in the calculation. Blue: Si, Red: O and Green: position of the M ion corresponding to the crystallographic site T1.

3. Experimental Details

Copper- and Manganese-containing BEA zeolites were prepared from parent TEABEA zeolite by a two-step postsynthesis method [40–44]. In the first step, TEABEA zeolite (Si/Al = 17) was dealuminated by a treatment with nitric acid solution of C = 13 mol L^{-1} at 353 K for 4 h, to obtain

aluminum free SiBEA zeolite, and then it was washed several times with distilled water and dried at 368 K overnight.

In the second step SiBEA zeolites were put in contact with $Cu(NO_3)_2$ or $Mn(NO_3)_2$ aqueous solution with appropriate concentration and stirred for 24 h at 298 K. Then, the suspensions were stirred in evaporator under vacuum of a water pump for 2 h at 333 K until the water was evaporated. The obtained materials with Cu and Mn atoms in the framework position were denoted as Cu2.0SiBEA or Mn2.0SiBEA where number next to element symbol refers to Cu or Mn wt % content.

4. Results and discussion

4.1 Geometric and energetic analysis

The Cu and Mn atoms were substituted for the Si in the BEA framework at the T1 site thus leading to CuSiBEA and MnSiBEA. The number of substitutions in m% is 1.64 and 1.42, respectively, for CuSiBEA and MnSiBEA and the Si/M ratio is equal to 63 for both. The difference between these rates is due to the difference of molar mass of both atoms. The introduction of a M^{2+} ion in a zeolite framework causes a charge deficit that must be compensated for the neutrality of the system, achieved by incorporating 2 H^+. The protons may bind to lattice oxygen sites forming of hydroxyl groups, in contrast with M ions with higher oxidation states for which oxo-groups can be introduced (See refs [4,6,37–39]). The hydroxyl groups surrounding the M center can be organized as shown in Figure 2, leading to 6 isomers that have been considered in the present work.

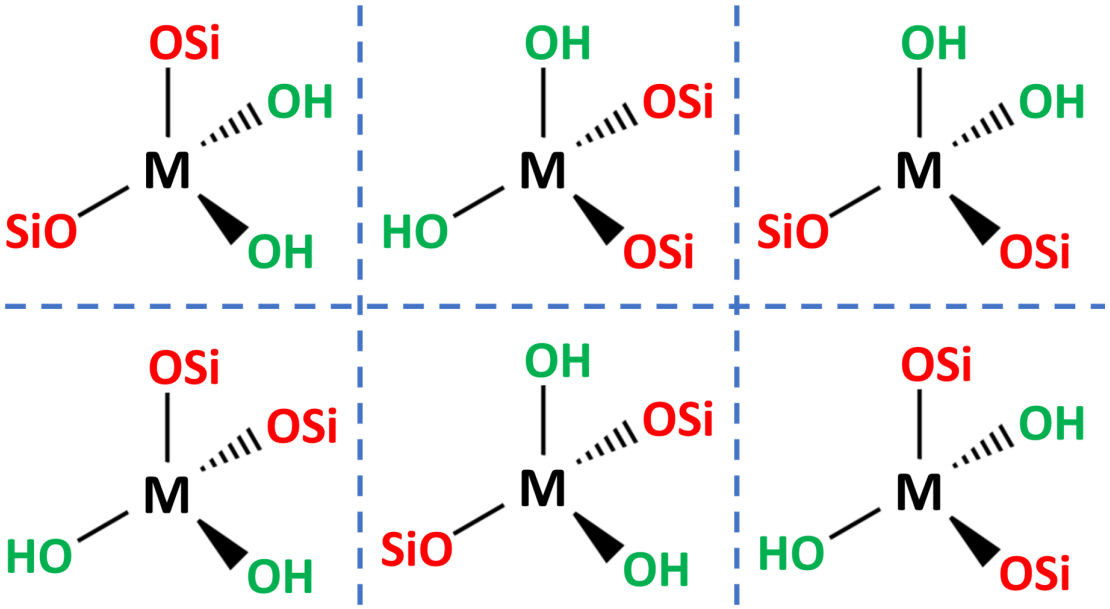

Figure 2. Different isomers of MSiBEA (M = Cu and Mn) with surrounded groups OSi (in red) and OH (in green).

The Si atoms of the two OSi groups which are linked to the transition metal do not have the same chemical environment (T2, T3, T7 and T8) and it is the same for two silanol groups. Accordingly, we choose to name the different isomers by the site of the two silanol groups as follow: T2-T3, T2-T7, T2-T8, T3-T7 and T7-T8 i.e. T2-T3 represents the configuration in which OH groups are linked to the silicon atoms located in site T2 and T3. For each isomer, we have investigated several orientations to the 2 H^+ of the 2 OH groups and only the most stable one is reported.

The optimized structures of the six CuSiBEA isomers are displayed in Figure 3 while Table 1 shows the geometric parameters and the relative total energies calculated for CuSiBEA. Copper fits into the framework with a coordination number II making two Cu-OSi bonds. The first varies between 1.78 and 1.81 Å while the second between 1.81 and 1.88 Å. These two bonds are on average 1.82 Å. They exceed the classical Si-O bonds in zeolites whose average value is 1.64 Å. This difference can be explained by the difference in size of these two elements whose ionic radii are 40 and 78 pm, respectively, for Si^{4+} and Cu^{2+}. The M-OSi distances are then proportional to the size of the metals. From the orientation of the surrounding silanol groups one can conclude that copper also interacts weakly with them. The calculated Cu-OH distances vary between 2.0 and 2.87 Å with an average value of 2.25 Å. The O-H distances of the two hydroxyl groups vary very weakly between 0.97 and 1.0 Å. The O-Cu-O bridge varies widely depending on the configurations between 130 and 160 °. The

average value calculated over all the configurations is 147°. This value is well above the average of the calculated O-Si-O angle (110°).

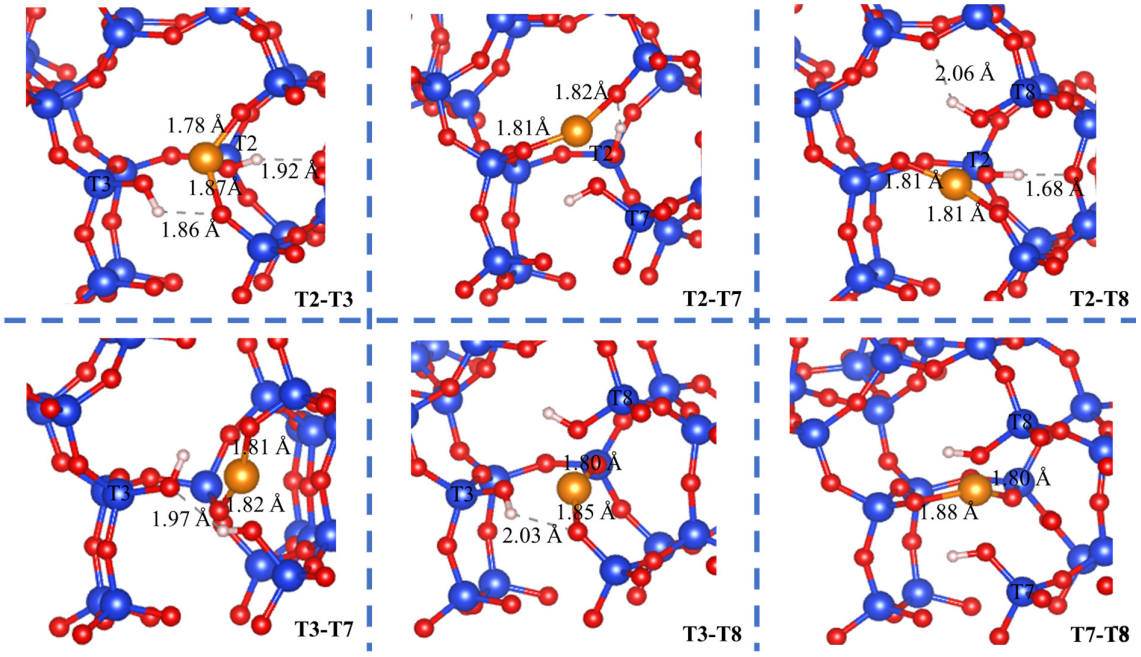

Figure 3. Optimized geometries of CuSiBEA (Cu atom in gold). Cu-O and H-bond distances are displayed.

The calculated relative energy for CuSiBEA is in range of 0 to 0.21 eV. This parameter is used to classify the six configurations in order of decreasing stability as follows: T3-T7 > T7-T8 > T3-T8 > T2-T7 > T2-T8 > T2-T3. Here the most stable configuration is the T3-T7 unlike Mn-BEA where it is rather the most stable T7-T8. However, the energy difference between T3-T7 and T7-T8 is quite low (0.02 eV) for Cu-BEA then one can consider T3-T7 ≈ T7-T8.

Table 1. Geometric parameters and relative energies of the different Cu(II)SiBEA configurations studied. When two values are available, they are presented by v1/v2 where v1 is the first value and v2 the second. Distances in Å, Angles in ° and Energies in eV.

Cu(II)SiBEA	Cu-OSi	Cu-OH	Si-OH	O-H	$\widehat{OCuO}$	ΔE_{rel}
T2-T3	1.777/1.870	1.991/2.601	1.641/1.673	0.982/0.998	130.2	0.21
T2-T7	1.814/1.819	2.009/2.761	1.634/1.685	0.984/0.992	155.6	0.11
T2-T8	1.809/1.810	2.046/2.279	1.646/1.669	0.980/0.998	152.5	0.19
T3-T7	1.812/1.824	2.046/2.774	1.651/1.663	0.979/0.983	159.5	0.00
T3-T8	1.797/1.848	2.135/2.264	1.658/1.665	0.977/0.985	148.2	0.08
T7-T8	1.799/1.878	2.008/2.358	1.640/1.672	0.975/0.976	138.3	0.02

Concerning MnSiBEA, we have considered the same configuration as those used for CuSiBEA. The optimized geometries for MnSiBEA are shown in Figure 4.

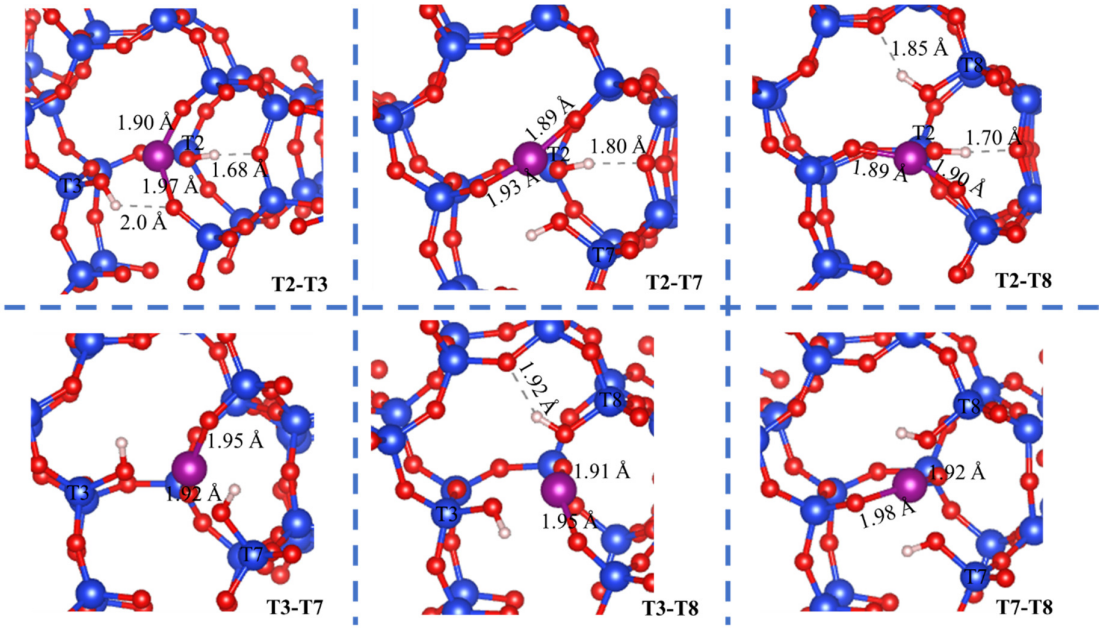

Figure 4. Optimized geometries of MnSiBEA (Mn atom in purple). Mn-O and H-bond distances are displayed.

The geometric parameters and the relative energies calculated for MnSiBEA are reported in

Table 2. By substituting the silicon with the manganese, two Mn-O(Si) bonds are formed with lengths varying between 1.89 and 1.98 Å with an average value of 1.93 Å. The two other oxygen atoms located in the vicinity of the metal (Mn) are now involved in two silanol obtained by adding two H^+ protons. These oxygen atoms are less close to the metal (Mn) compared to the two previous ones with Mn-O(H) distances varying in range of 2.16 to 2.29 Å (an average of 2.21 Å). We notice that Mn-OSi are slightly larger than Cu-OSi and this even though the ionic radius of Mn^{2+} (67 pm) is smaller than that of Cu^{2+} (73 pm) Cu. Regarding the O-H distances, they vary weakly between 0.97 and 1 Å with an average value of 0.99 Å. Si-OH distances are quite similar for all configurations with an average value of 1.67 Å. The calculated OMnO angles vary widely between 124 and 153° with an average value of 143°.

The relative energies calculated for MnSiBEA vary between 0 and 0.29 eV. With these relative energies, the six configurations can be classified in terms of stability as follow: T7-T8 > T3-T7 > T3-

T8 > T2-T7 > T2-T8 > T2-T3. The most stable configuration (T7-T8) displays 145 ° for OMnO angle while the least stable configuration (T2-T3) displays 124 ° for the OMnO angle.

Table 2. Geometric parameters and relative energies of the different Mn(II)SiBEA configurations studied. When two values are available, they are presented by v1/v2 where v1 is the first value and v2 the second. Distances in Å, Angles in ° and Energies in eV.

Mn(II)SiBEA	Mn-OSi	Mn-OH	Si-OH	O-H	$\widehat{OMnO}$	ΔE_{rel}
T2-T3	1.896/1.969	2.182/2.204	1.661/1.662	0.992/1.001	124	0.29
T2-T7	1.893/1.934	2.233/2.288	1.657/1.665	0.983/0.993	153.2	0.09
T2-T8	1.893/1.897	2.176/2.231	1.661/1.663	0.989/0.994	149.8	0.23
T3-T7	1.918/1.946	2.188/2.206	1.670/1.672	0.977/0.986	145.9	0.02
T3-T8	1.913/1.948	2.164/2.241	1.665/1.676	0.981/0.985	137.8	0.06
T7-T8	1.923/1.978	2.179/2.193	1.663/1.673	0.975/0.980	145.0	0.00

The total substitution reaction energy is estimated following the reaction:

$$SiBEA + MH_2 \rightarrow MBEAH_2 + Si$$

with MH_2 and Si in the gas phase. The reaction energy was calculated to be equal to 6.9 and 5.5 eV, for Cu^{2+} and Mn^{2+} respectively. These values, calculated at 0 K, show that the substitution is an endothermic reaction. The substitution energy of Cu^{2+} is 0.6 eV higher than that of Mn^{2+}. Accordingly, one can conclude that the substitution should be easiest for Mn^{2+} than Cu^{2+}.

4.2 Frequencies analysis

Calculated vibrational frequencies of CuSiBEA for all configurations were reported in Table 3. The accuracy of the calculated frequencies was found to be within 75 cm^{-1} for the high wave number OH vibrations, and a few cm^{-1} for the Metal-O vibrations around 1000 cm^{-1} [80–82]. The analysis of each spectrum obtained shows two peaks corresponding to OH stretching ranging from 3215 to 3725 cm^{-1}. The shift between these two peaks varies from 40 to 395 cm^{-1}. The smallest deviation is obtained with the T7-T8 configuration while the largest deviation (395 cm^{-1}) is observed with the T7-T8 configuration. The most stable configuration (T3-T7) has 140 cm^{-1} between both peaks.

The peaks that can be attributed to the vibrations of SiO (H) elongations are observed around 800-900 cm^{-1} for the six configurations. Regarding CuO elongation vibrations, they are between 500 and 700 cm^{-1}. The calculated IR spectra for the most stable configuration is displayed in Figure 5.

Table 3. Calculated vibrational frequencies of CuSiBEA with possible assignment. Frequencies in cm^{-1}. str=stretching, rock=rocking modes

T2-T3	T2-T7	T2-T8	T3-T7	T3-T8	T7-T8	Experiment	Assignment
3536.6	3547.6	3609.0	3627.3	3678.8	3722.6	3733	OH str
3300	3303.9	3214.1	3547.6	3536.4	3683.1	3540	OH str
1172.1	1190.7	1183.9	1179.4	1171.9	1175		SiO str
1157.9	1177.2	1162.9	1154.4	1167.3	1161.5	968	SiO str
1052.7	1036.2	989.0	984	974.5	914.1	-	OH rock
1028.9	983.8	512.8	944.6	905.2	-	-	OH rock
990.9	963.9	1048.8	922.2	1012.8	1002.5	-	SiO(Cu) str
959.1	940.4	1037.3	838.4	964.7	957.3	-	SiO(Cu) str
887.7	888.5	881.6	916.1	863.2	825.1	810	SiO(H) str
835.3	808.6	839.3	818.8	831.8	786.4	744	SiO(H) str
608.8	665.5	613.8	659.3	689.7	665	580	CuO str
484.6	435.4	520.4	546.5	543.1	502.1	525	CuO str

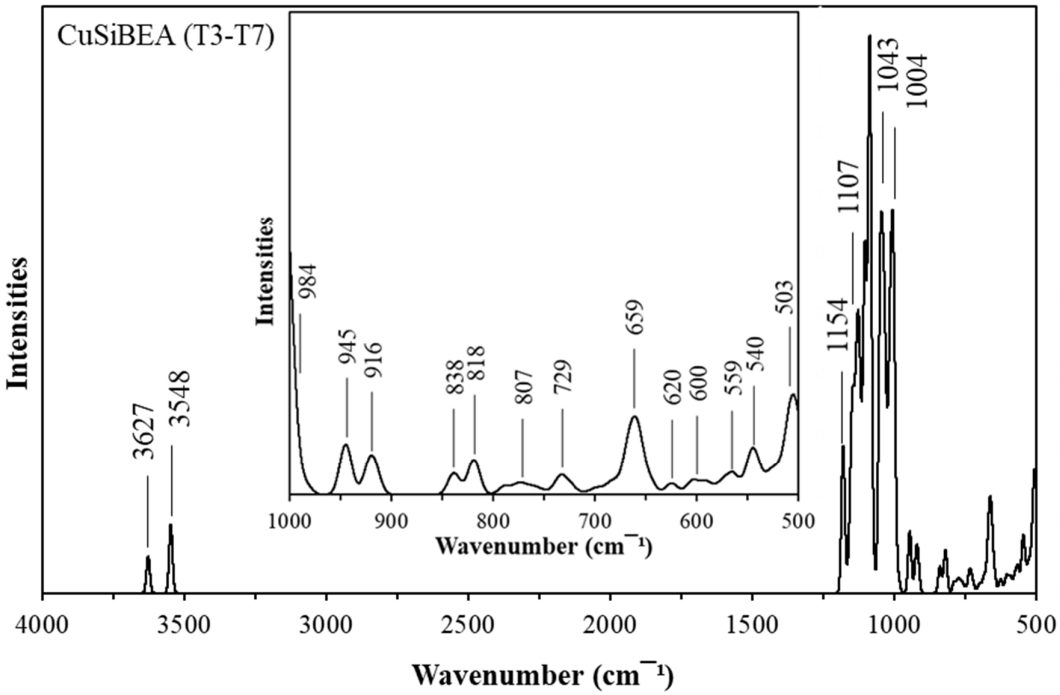

Figure 5. Calculated IR spectrum for the CuSiBEA zeolite obtained in the range 500 – 4000 cm^{-1}. Assignments in Table 3.

We have reported in **Table 4** the calculated vibrational frequencies of MnSiBEA for the six configurations. All the calculated IR spectra show two peaks between 3740 and 3150 cm^{-1}. These two peaks correspond to the vibrations of elongations of the two hydroxyl groups. They are separated by a difference ranging from 113 to 250 cm^{-1}, which makes it possible to confirm without ambiguity the presence of the two hydroxyl groups in the framework. Of the two OH peaks, the peak with the greater frequency corresponds to the hydroxyl group bonded to the T (Si) atom of the higher site. This suggests that the frequency of vibration of OH elongation strongly depends on the site T where this group is located. Peaks located between 3200 and 3550 cm^{-1} can be associated with hydroxyl groups involved in hydrogen bonds [40,83,84]. The most stable configuration (T7-T8) predicted by relative energies displays these two peaks at frequencies 3735 and 3623 cm^{-1} while the least stable configuration (T2-T3) displays its two OH peaks at frequencies 3412 and 3163 cm^{-1}. A large range without any vibration is present on all configurations. It ranges from 1195 to 3160 cm^{-1} for the least stable configuration and from 1175 to 3620 cm^{-1} for the most stable configuration. The area from 1000 to 1190 cm^{-1} corresponds to the vibrations of SiO elongations. The vibrations of deformations of OH groups are between 800 and 1000 cm^{-1}. The vibrations of SiO elongations of the silanols are also observed in this range. Similar values are reported in Table 3 for CuSiBEA. The peaks corresponding to MnO vibrations are located at 580 and 660 cm^{-1}. The vibration frequencies and vibration modes

calculated for both MnSiBEA and CuSiBEA are quite similar despite the significant difference in size between Mn and Cu. Figure 6 displays the calculated IR spectrum of MnSiBEA.

Table 4. Calculated vibrational frequencies of MnSiBEA with possible assignment. Frequencies in cm^{-1}. str=stretching, rock=rocking modes

T2-T3	T2-T7	T2-T8	T3-T7	T3-T8	T7-T8	Experiment	Assignment
3412.6	3558.6	3422.8	3687.3	3619.9	3735	3733	OH str
3163.1	3351	3290.2	3512.2	3501.1	3622.7	3540	OH str
1191	1176.8	1179.6	1158.5	1167.2	1170.7	-	SiO str
1166.8	1162.1	1166	1150.1	1165.3	1163.6	968	SiO str
996.7	967.8	806.4	1000.9	1004.7	957.9	-	OH rock
804.2	930.9	594.7	969.1	930.4	911	-	OH rock
868.5	867.2	868.8	847.1	853.8	855.8	810	SiO(H) str
857.3	850.8	853.2	833.4	829.5	831.4	744	SiO(H) str
657.7	659.9	-	-	668.3	665.2	625	MnO str
620.7	647.9	-	-	620.7	636.8	580	MnO str

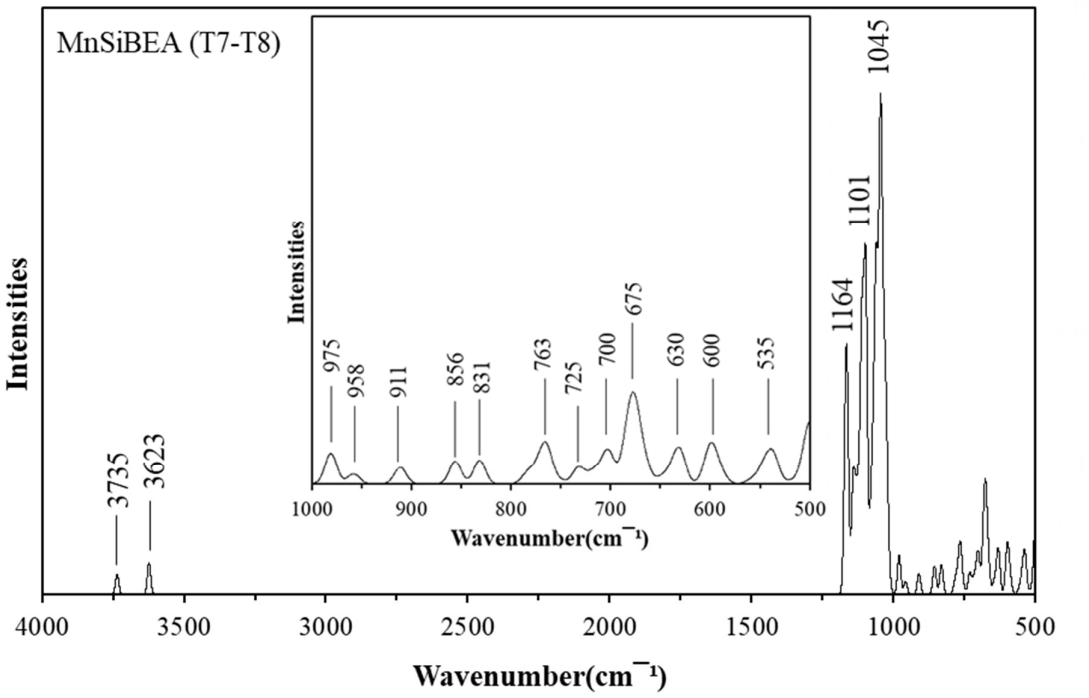

Figure 6. Calculated IR spectrum for the MnSiBEA zeolite obtained in the range 500 – 4000 cm^{-1}. Assignments in Table 4.

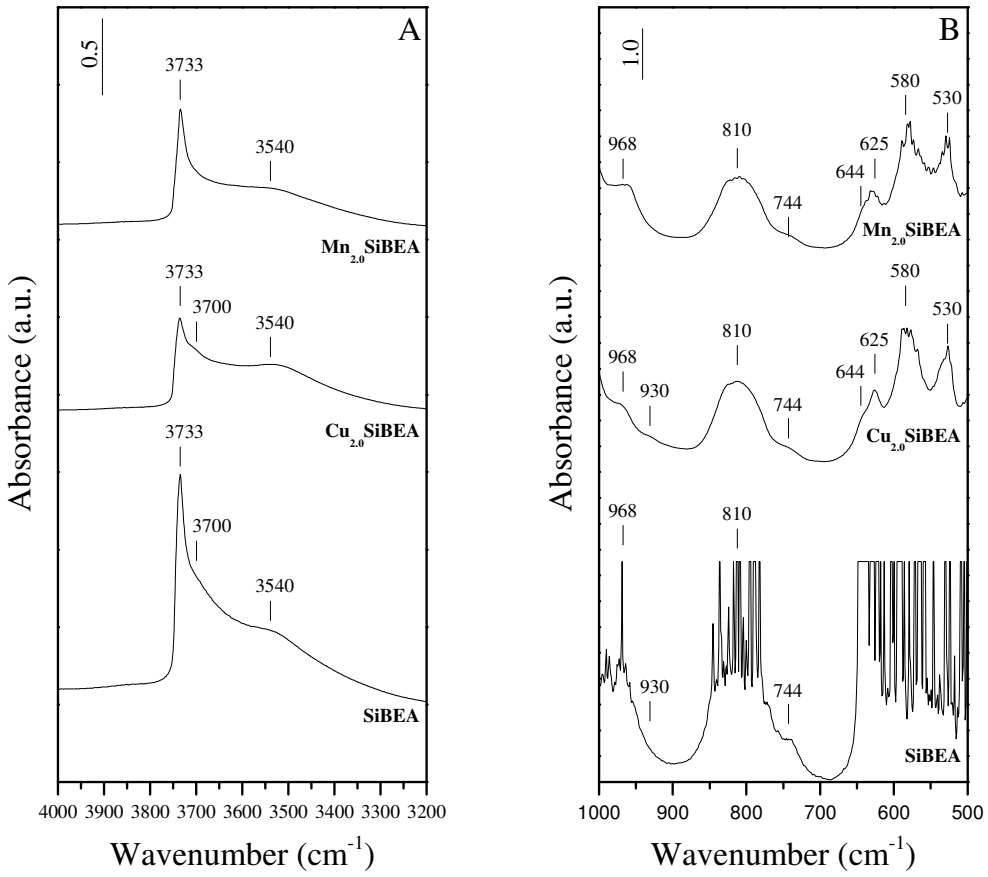

Figure 7. Experimental IR spectra of Mn2.0SiBEA (A), Cu2.0SiBEA and SiBEA in the range of OH groups (4000-3200) (A) and M-O groups (1000-500 cm-1) (B) is shown.

The **Figure 7** shows the experimental IR spectra of $Cu_{2.0}$SiBEA, $Mn_{2.0}$SiBEA and SiBEA in the range of OH groups (4000-3200 cm^{-1}) (A) and structural vibration of BEA zeolite (1000 – 500 cm^{-1}) (B). Both spectra ($Cu_{2.0}$SiBEA and $Mn_{2.0}$SiBEA) are similar, proof that the incorporation of Cu^{2+} and Mn^{2+} into the framework of the zeolite succeed without any modification of the framework. This is also supported by the IR spectrum of pure SiBEA ~~(Figure7). that can be found as Supporting Information.~~ Stretching vibrations of OH appear at 3540 and 3733 cm^{-1} supporting the presence of hydroxyl groups. By comparing experimental and theoretical spectra, in the range of 4000-3200 cm^{-1}, a very nice agreement is observed. Experimental peak at 968 cm^{-1} for CuSiBEA and MnSiBEA can be attributed to Si-O stretching. Si-O(H) vibrations are around 810 cm^{-1} while Cu-O an Mn-O peaks are

in a range of 500-650 cm^{-1}. Difference seen in this range between CuSiBEA and MnSiBEA can be due to the formation of Cu-O and Mn-O bonds. However, considering the complexity of the system and the calculation level, theoretical results are found to be in very good agreement with experiment, allowing an ab initio assignment of the bands observed.

Conclusions

In this study, we describe the incorporation of copper (II) and manganese (II) in vacant T atom sites of SiBEA zeolite. This process leads to the formation of 6 possible isomers, involving the formation of hydroxyl groups in different lattice positions. An energetic analysis made it possible to identify the most stable isomer in each of the two models. The IR spectra are calculated and compared with those determined experimentally. The spectra of the M-modified zeolites are very similar to the pure SiBEA system, indicating that the incorporation reaction was reached without modification of the framework. Experimental spectra are resolved and associated with molecular vibrations and site geometry. No experimental vibrations were detected between 1100 and 3100 cm^{-1}. OH vibrations are obtained around 3500 and 3700 cm^{-1}. CuO(Si) vibrations are found around 600 cm^{-1} as well as MnO(Si) vibrations with a slight difference. Both CuO(H) and MnO(H) overlap with SiO(H) bands around 1000 cm^{-1}. Theoretical results are in nice agreement with experimental ones, providing the localization and speciation of the potential catalytic sites generated by the incorporation of Cu^{2+} and Mn^{2+} in the zeolite framework. Finally, it is also shown that the accurate molecular description of the active sites is important for understanding the catalysis going on and for developing novel catalytic processes.

~~Supporting information~~

~~IR spectra of the pure and M-modified SiBEA materials~~

Acknowledgements

E.H. is grateful to the VUB-ALGC group and to the Global Minds project (Benin – VUB) for financial support. This work was granted access to the HPC resources of TGCC under the allocations 2020- A0080810433 and 2021-A0100810433 by GENCI-EDARI project. Computational resources and services were also provided by the Shared ICT Services Centre funded by the Vrije Universiteit Brussel, the Flemish Supercomputer Center (VSC) and FWO. FT wishes to acknowledge the VUB for support, among other through a Strategic Research Program awarded to his group. F.T. is also grateful to the Université de Lorraine for a one-month visiting professorship in 2019 and 2020.

References

[1] B. Notari, Microporous Crystalline Titanium Silicates, in: D.D. Eley, W.O. Haag, B. Gates (Eds.), Advances in Catalysis, Academic Press, 1996: pp. 253–334. https://doi.org/10.1016/S0360-0564(08)60042-5.
[2] A. Corma, From microporous to mesoporous molecular sieve materials and their use in catalysis, Chemical Reviews. 97 (1997) 2373–2420.
[3] F. Tielens, S. Dzwigaj, Group V metal substitution in silicate model zeolites: In search for the active site, Chemical Physics Letters. 501 (2010) 59–63.
[4] F. Tielens, T. Shishido, S. Dzwigaj, What Do the Niobium Framework Sites Look Like in Redox Zeolites? A Combined Theoretical and Experimental Investigation, J. Phys. Chem. C. 114 (2010) 3140–3147. https://doi.org/10.1021/jp910956j.
[5] F. Tielens, S. Dzwigaj, Probing acid–base sites in vanadium redox zeolites by DFT calculation and compared with FTIR results, Catalysis Today. 152 (2010) 66–69.
[6] A. Wojtaszek, M. Ziolek, S. Dzwigaj, F. Tielens, Comparison of competition between T=O and T–OH groups in vanadium, niobium, tantalum BEA zeolite and SOD based zeolites, Chemical Physics Letters. 514 (2011) 70–73. https://doi.org/10.1016/j.cplett.2011.08.005.
[7] F. Tielens, M.M. Islam, G. Skara, F. De Proft, T. Shishido, S. Dzwigaj, Chromium sites in zeolite framework: Chromyl or chromium hydroxyl groups?, Microporous and Mesoporous Materials. 159 (2012) 66–73.
[8] J. Handzlik, R. Grybos, F. Tielens, Structure of monomeric chromium (VI) oxide species supported on silica: periodic and cluster DFT studies, The Journal of Physical Chemistry C. 117 (2013) 8138–8149.
[9] J. Handzlik, R. Grybos, F. Tielens, Isolated chromium (VI) oxide species supported on Al-modified silica: a molecular description, The Journal of Physical Chemistry C. 120 (2016) 17594–17603.
[10] B.M. Weckhuysen, R.A. Schoonheydt, Olefin polymerization over supported chromium oxide catalysts, Catalysis Today. (1999) 7.
[11] K. Chen, A.T. Bell, E. Iglesia, Kinetics and Mechanism of Oxidative Dehydrogenation of Propane on Vanadium, Molybdenum, and Tungsten Oxides, J. Phys. Chem. B. 104 (2000) 1292–1299. https://doi.org/10.1021/jp9933875.
[12] M.A. Bañares, Supported metal oxide and other catalysts for ethane conversion: a review, Catalysis Today. 51 (1999) 319–348. https://doi.org/10.1016/S0920-5861(99)00053-X.
[13] G. Deo, I.E. Wachs, Reactivity of supported vanadium oxide catalysts: The partial oxidation of methanol, Journal of Catalysis. 146 (1994) 323–334.

[14] S. Gueddida, S. Lebègue, M. Badawi, Interaction between transition metals (Co, Ni, and Cu) systems and amorphous silica surfaces: A DFT investigation, Applied Surface Science. 533 (2020) 147422. https://doi.org/10.1016/j.apsusc.2020.147422.
[15] P. Boroń, L. Chmielarz, J. Gurgul, K. Lątka, B. Gil, B. Marszalek, S. Dzwigaj, Influence of iron state and acidity of zeolites on the catalytic activity of FeHBEA, FeHZSM-5 and FeHMOR in SCR of NO with NH3 and N2O decomposition, Microporous and Mesoporous Materials. 203 (2015) 73–85.
[16] S. Dzwigaj, N. Popovych, P. Kyriienko, J.-M. Krafft, S. Soloviev, The similarities and differences in structural characteristics and physico-chemical properties of AgAlBEA and AgSiBEA zeolites, Microporous and Mesoporous Materials. 182 (2013) 16–24. https://doi.org/10.1016/j.micromeso.2013.08.009.
[17] P.I. Kyriienko, O.V. Larina, S.O. Soloviev, S.M. Orlyk, S. Dzwigaj, High selectivity of TaSiBEA zeolite catalysts in 1, 3-butadiene production from ethanol and acetaldehyde mixture, Catalysis Communications. 77 (2016) 123–126.
[18] P.I. Kyriienko, O.V. Larina, S.O. Soloviev, S.M. Orlyk, C. Calers, S. Dzwigaj, Ethanol conversion into 1, 3-butadiene by the Lebedev method over MTaSiBEA zeolites (M= Ag, Cu, Zn), ACS Sustainable Chemistry & Engineering. 5 (2017) 2075–2083.
[19] P.I. Kyriienko, O.V. Larina, N.O. Popovych, S.O. Soloviev, Y. Millot, S. Dzwigaj, Effect of the niobium state on the properties of NbSiBEA as bifunctional catalysts for gas-and liquid-phase tandem processes, Journal of Molecular Catalysis A: Chemical. 424 (2016) 27–36.
[20] N.O. Popovych, O.V. Larina, S.M. Orlyk, P.I. Kyriienko, S.O. Soloviev, S. Dzwigaj, Design of Bifunctional Catalysts Based on Bea Zeolites for Tandem Processes with Participation of Ethanol, Theoretical and Experimental Chemistry. 54 (2018) 255–264.
[21] M. Trejda, M. Ziolek, Y. Millot, K. Chalupka, M. Che, S. Dzwigaj, Methanol oxidation on VSiBEA zeolites: Influence of V content on the catalytic properties, Journal of Catalysis. 281 (2011) 169–176.
[22] S. Grundner, Single-site trinuclear copper oxygen clusters in mordenite for selective conversion of methane to methanol, NATURE COMMUNICATIONS. (2015) 9.
[23] S. Grundner, Synthesis of single-site copper catalysts for methane partial oxidation, (2016) 4.
[24] P. Vanelderen, B.E.R. Snyder, M.-L. Tsai, R.G. Hadt, J. Vancauwenbergh, O. Coussens, R.A. Schoonheydt, B.F. Sels, E.I. Solomon, Spectroscopic Definition of the Copper Active Sites in Mordenite: Selective Methane Oxidation, J. Am. Chem. Soc. (2015) 10.
[25] Z. Qin, S. Zeng, G. Melinte, T. Bučko, M. Badawi, Y. Shen, J.-P. Gilson, O. Ersen, Y. Wei, Z. Liu, Understanding the Fundamentals of Microporosity Upgrading in Zeolites: Increasing Diffusion and Catalytic Performances, Advanced Science. (2021) 2100001.
[26] S. Komaty, A. Daouli, M. Badawi, C. Anfray, M. Zaarour, S. Valable, S. Mintova, Incorporation of trivalent cations in NaX zeolite nanocrystals for the adsorption of O 2 in the presence of CO 2, Physical Chemistry Chemical Physics. 22 (2020) 9934–9942.
[27] I. Khalil, H. Jabraoui, G. Maurin, S. Lebègue, M. Badawi, K. Thomas, F. Mauge, Selective capture of phenol from biofuel using protonated faujasite zeolites with different Si/Al ratios, The Journal of Physical Chemistry C. 122 (2018) 26419–26429.
[28] Q. Lin, J. Li, L. Ma, J. Hao, Selective catalytic reduction of NO with NH3 over Mn–Fe/USY under lean burn conditions, Catalysis Today. 151 (2010) 251–256. https://doi.org/10.1016/j.cattod.2010.01.026.
[29] A. Sultana, M. Sasaki, H. Hamada, Influence of support on the activity of Mn supported catalysts for SCR of NO with ammonia, Catalysis Today. 185 (2012) 284–289.
[30] M. Stanciulescu, G. Caravaggio, A. Dobri, J. Moir, R. Burich, J.-P. Charland, P. Bulsink, Low-temperature selective catalytic reduction of NOx with NH3 over Mn-containing catalysts, Applied Catalysis B: Environmental. 123–124 (2012) 229–240. https://doi.org/10.1016/j.apcatb.2012.04.012.

[31] T. Komatsu, M. Nunokawa, I.S. Moon, T. Takahara, S. Namba, T. Yashima, Kinetic Studies of Reduction of Nitric Oxide with Ammonia on Cu2+-Exchanged Zeolites, Journal of Catalysis. 148 (1994) 427–437. https://doi.org/10.1006/jcat.1994.1229.
[32] M. Colombo, I. Nova, E. Tronconi, A comparative study of the NH3-SCR reactions over a Cu-zeolite and a Fe-zeolite catalyst, Catalysis Today. 151 (2010) 223–230.
[33] Y. Meng, H.C. Genuino, C.-H. Kuo, H. Huang, S.-Y. Chen, L. Zhang, A. Rossi, S.L. Suib, One-step hydrothermal synthesis of manganese-containing MFI-type zeolite, Mn–ZSM-5, characterization, and catalytic oxidation of hydrocarbons, Journal of the American Chemical Society. 135 (2013) 8594–8605.
[34] H. Einaga, S. Futamura, Catalytic oxidation of benzene with ozone over Mn ion-exchanged zeolites, Catalysis Communications. 8 (2007) 557–560. https://doi.org/10.1016/j.catcom.2006.07.024.
[35] B.-Z. Zhan, B. Modén, J. Dakka, J.G. Santiesteban, E. Iglesia, Catalytic oxidation of n-hexane on Mn-exchanged zeolites: Turnover rates, regioselectivity, and spatial constraints, Journal of Catalysis. 245 (2007) 316–325.
[36] S. Dzwigaj, Y. Millot, M. Che, Ta (V)-single site BEA zeolite by two-step postsynthesis method: preparation and characterization, Catalysis Letters. 135 (2010) 169–174.
[37] F. Tielens, M. Calatayud, S. Dzwigaj, M. Che, What do vanadium framework sites look like in redox model silicate zeolites?, Microporous and Mesoporous Materials. 119 (2009) 137–143. https://doi.org/10.1016/j.micromeso.2008.10.007.
[38] D.C. Tranca, F.J. Keil, I. Tranca, M. Calatayud, S. Dzwigaj, M. Trejda, F. Tielens, Methanol Oxidation to Formaldehyde on VSiBEA Zeolite: A Combined DFT/vdW/Transition Path Sampling and Experimental Study, J. Phys. Chem. C. 119 (2015) 13619–13631. https://doi.org/10.1021/acs.jpcc.5b01911.
[39] F. Tielens, T. Shishido, S. Dzwigaj, What do tantalum framework sites look like in zeolites? A combined theoretical and experimental investigation, The Journal of Physical Chemistry C. 114 (2010) 9923–9930.
[40] S. Dzwigaj, M.J. Peltre, P. Massiani, A. Davidson, M. Che, T. Sen, S. Sivasanker, Incorporation of vanadium species in a dealuminated β zeolite, Chemical Communications. (1998) 87–88.
[41] S. Dzwigaj, M. Matsuoka, R. Franck, M. Anpo, M. Che, Probing different kinds of vanadium species in the VSiβ zeolite by diffuse reflectance UV- visible and photoluminescence spectroscopies, The Journal of Physical Chemistry B. 102 (1998) 6309–6312.
[42] S. Dzwigaj, P. Massiani, A. Davidson, M. Che, Role of Silanol Groups in the Incorporation of V in β Zeolite, Journal of Molecular Catalysis A: Chemical. 155 (2000) 169–182.
[43] S. Dzwigaj, Recent advances in the incorporation and identification of vanadium species in microporous materials, Current Opinion in Solid State and Materials Science. 7 (2003) 461–470. https://doi.org/10.1016/j.cossms.2004.03.011.
[44] S. Dzwigaj, E. Ivanova, R. Kefirov, K. Hadjiivanov, F. Averseng, J.M. Krafft, M. Che, Remarkable effect of the preparation method on the state of vanadium in BEA zeolite: Lattice and extra-lattice V species, Catalysis Today. 142 (2009) 185–191. https://doi.org/10.1016/j.cattod.2008.09.031.
[45] S. Dzwigaj, J. Janas, J. Gurgul, R.P. Socha, T. Shishido, M. Che, Do Cu(II) ions need Al atoms in their environment to make CuSiBEA active in the SCR of NO by ethanol or propane? A spectroscopy and catalysis study, Applied Catalysis B: Environmental. 85 (2009) 131–138. https://doi.org/10.1016/j.apcatb.2008.07.003.
[46] R. Baran, F. Averseng, D. Wierzbicki, K. Chalupka, J.-M. Krafft, T. Grzybek, S. Dzwigaj, Effect of postsynthesis preparation procedure on the state of copper in CuBEA zeolites and its catalytic properties in SCR of NO with NH3, Applied Catalysis A: General. 523 (2016) 332–342. https://doi.org/10.1016/j.apcata.2016.06.008.

[47] G. Moretti, C. Dossi, A. Fusi, S. Recchia, R. Psaro, A comparison between Cu-ZSM-5, Cu–S-1 and Cu–mesoporous-silica–alumina as catalysts for NO decomposition, Applied Catalysis B: Environmental. 20 (1999) 67–73. https://doi.org/10.1016/S0926-3373(98)00096-4.
[48] M.H. Groothaert, P.J. Smeets, B.F. Sels, P.A. Jacobs, R.A. Schoonheydt, Selective Oxidation of Methane by the Bis(μ-oxo)dicopper Core Stabilized on ZSM-5 and Mordenite Zeolites, J. Am. Chem. Soc. 127 (2005) 1394–1395. https://doi.org/10.1021/ja047158u.
[49] H. Praliaud, S. Mikhailenko, Z. Chajar, M. Primet, Surface and bulk properties of Cu–ZSM-5 and Cu/Al2O3 solids during redox treatments. Correlation with the selective reduction of nitric oxide by hydrocarbons, Applied Catalysis B: Environmental. 16 (1998) 359–374. https://doi.org/10.1016/S0926-3373(97)00093-3.
[50] I. Lezcano-Gonzalez, U. Deka, H.E. van der Bij, P. Paalanen, B. Arstad, B.M. Weckhuysen, A.M. Beale, Chemical deactivation of Cu-SSZ-13 ammonia selective catalytic reduction (NH3-SCR) systems, Applied Catalysis B: Environmental. 154–155 (2014) 339–349. https://doi.org/10.1016/j.apcatb.2014.02.037.
[51] A. Godiksen, F.N. Stappen, P.N.R. Vennestrøm, F. Giordanino, S.B. Rasmussen, L.F. Lundegaard, S. Mossin, Coordination Environment of Copper Sites in Cu-CHA Zeolite Investigated by Electron Paramagnetic Resonance, J. Phys. Chem. C. 118 (2014) 23126–23138. https://doi.org/10.1021/jp5065616.
[52] J. Soria, A. Martı&nez-Arias, A. Martı&nez-Chaparro, J.C. Conesa, Z. Schay, Influence of the Preparation Method, Outgassing Treatment, and Adsorption of NO and/or O2 on the Cu2+ Species in Cu-ZSM-5: An EPR Study, Journal of Catalysis. 190 (2000) 352–363. https://doi.org/10.1006/jcat.1999.2750.
[53] S.C. Larsen, A. Aylor, A.T. Bell, J.A. Reimer, Electron Paramagnetic Resonance Studies of Copper Ion-Exchanged ZSM-5, J. Phys. Chem. 98 (1994) 11533–11540. https://doi.org/10.1021/j100095a039.
[54] C.E. Sass, L. Kevan, Comparative electron spin echo study of aluminum modulation associated with copper (2+) in Ca-ZSM-5 and K-ZSM-5 zeolites, The Journal of Physical Chemistry. 92 (1988) 14–15.
[55] P.J. Carl, S.C. Larsen, Variable-temperature electron paramagnetic resonance studies of copper-exchanged zeolites, Journal of Catalysis. 182 (1999) 208–218.
[56] J. Janas, T. Machej, J. Gurgul, R.P. Socha, M. Che, S. Dzwigaj, Effect of Co content on the catalytic activity of CoSiBEA zeolite in the selective catalytic reduction of NO with ethanol: Nature of the cobalt species, Applied Catalysis B: Environmental. 75 (2007) 239–248.
[57] A. Corma, A. Palomares, F. Márquez, Determining the Nature of the Active Sites of Cu-Beta Zeolites for the Selective Catalytic Reduction (SCR) of NOxby Using a Coupled Reaction-XAES/XPS Study, Journal of Catalysis. 170 (1997) 132–139. https://doi.org/10.1006/jcat.1997.1739.
[58] M. Narayana, S. Contarini, L. Kevan, X-ray photoelectron and electron spin resonance spectroscopic studies of Cu□NaY zeolites, Journal of Catalysis. 94 (1985) 370–375. https://doi.org/10.1016/0021-9517(85)90202-7.
[59] A.F. Wells, The lanthanides and actinides, in: Structural Inorganic Chemistry. 5. Ed, 1984.
[60] J.C. Bart, Near-edge X-ray absorption spectroscopy in catalysis, Advances in Catalysis. 34 (1986) 203–296.
[61] R. Baran, L. Valentin, S. Dzwigaj, Incorporation of Mn into the vacant T-atom sites of a BEA zeolite as isolated, mononuclear Mn: FTIR, XPS, EPR and DR UV-Vis studies, Physical Chemistry Chemical Physics. 18 (2016) 12050–12057.
[62] R. Baran, L. Valentin, J.-M. Krafft, T. Grzybek, P. Glatzel, S. Dzwigaj, Influence of the nature and environment of manganese in Mn-BEA zeolites on NO conversion in selective catalytic reduction with ammonia, Physical Chemistry Chemical Physics. 19 (2017) 13553–13561.
[63] G. Kresse, J. Hafner, Ab initio molecular dynamics for liquid metals, Phys. Rev. B. 47 (1993) 558–561. https://doi.org/10.1103/PhysRevB.47.558.

[64] G. Kresse, D. Joubert, From ultrasoft pseudopotentials to the projector augmented-wave method, Phys. Rev. B. 59 (1999) 1758–1775. https://doi.org/10.1103/PhysRevB.59.1758.
[65] B.S. Kulkarni, S. Krishnamurty, S. Pal, Influence of plane wave cut-off on structural and electronic properties in Sn-BEA and Ti-BEA zeolite water molecule interaction, Chemical Physics Letters. 484 (2010) 374–379.
[66] J.P. Perdew, K. Burke, M. Ernzerhof, Generalized gradient approximation made simple, Physical Review Letters. 77 (1996) 3865.
[67] S. Chibani, M. Chebbi, S. Lebègue, T. Bučko, M. Badawi, A DFT investigation of the adsorption of iodine compounds and water in H-, Na-, Ag-, and Cu- mordenite, J. Chem. Phys. 144 (2016) 244705. https://doi.org/10.1063/1.4954659.
[68] E.P. Hessou, W.G. Kanhounnon, D. Rocca, H. Monnier, C. Vallières, S. Lebègue, M. Badawi, Adsorption of NO, NO2, CO, H2O and CO2 over isolated monovalent cations in faujasite zeolite: a periodic DFT investigation, Theor Chem Acc. 137 (2018) 161. https://doi.org/10.1007/s00214-018-2373-2.
[69] F. Göltl, A. Grüneis, T. Bučko, J. Hafner, Van der Waals interactions between hydrocarbon molecules and zeolites: Periodic calculations at different levels of theory, from density functional theory to the random phase approximation and Møller-Plesset perturbation theory, J. Chem. Phys. 137 (2012) 114111. https://doi.org/10.1063/1.4750979.
[70] J.P.P. Ramalho, J.R. Gomes, F. Illas, Accounting for van der Waals interactions between adsorbates and surfaces in density functional theory based calculations: selected examples, RSC Advances. 3 (2013) 13085–13100.
[71] S. Grimme, J. Antony, S. Ehrlich, H. Krieg, A consistent and accurate ab initio parametrization of density functional dispersion correction (DFT-D) for the 94 elements H-Pu, J. Chem. Phys. 132 (2010) 154104. https://doi.org/10.1063/1.3382344.
[72] S. Grimme, S. Ehrlich, L. Goerigk, Effect of the damping function in dispersion corrected density functional theory, Journal of Computational Chemistry. 32 (2011) 1456–1465. https://doi.org/10.1002/jcc.21759.
[73] S. Baroni, S. De Gironcoli, A. Dal Corso, P. Giannozzi, Phonons and related crystal properties from density-functional perturbation theory, Reviews of Modern Physics. 73 (2001) 515.
[74] D. Karhánek, T. Bučko, J. Hafner, A density-functional study of the adsorption of methane-thiol on the (111) surfaces of the Ni-group metals: II. Vibrational spectroscopy, Journal of Physics: Condensed Matter. 22 (2010) 265006.
[75] I. Khalil, H. Jabraoui, S. Lebègue, W.J. Kim, L.-J. Aguilera, K. Thomas, F. Maugé, M. Badawi, Biofuel purification: Coupling experimental and theoretical investigations for efficient separation of phenol from aromatics by zeolites, Chemical Engineering Journal. 402 (2020) 126264. https://doi.org/10.1016/j.cej.2020.126264.
[76] Y. Foucaud, J. Lainé, L.O. Filippov, O. Barrès, W.J. Kim, I.V. Filippova, M. Pastore, S. Lebègue, M. Badawi, Adsorption mechanisms of fatty acids on fluorite unraveled by infrared spectroscopy and first-principles calculations, Journal of Colloid and Interface Science. 583 (2021) 692–703. https://doi.org/10.1016/j.jcis.2020.09.062.
[77] M. Gajdoš, K. Hummer, G. Kresse, J. Furthmüller, F. Bechstedt, Linear optical properties in the projector-augmented wave methodology, Physical Review B. 73 (2006) 045112.
[78] S. Shetty, B.S. Kulkarni, D.G. Kanhere, A. Goursot, S. Pal, A comparative study of structural, acidic and hydrophilic properties of Sn- BEA with Ti- BEA using periodic density functional theory, The Journal of Physical Chemistry B. 112 (2008) 2573–2579.
[79] J.M. Newsam, M.M.J. Treacy, W.T. Koetsier, C.B.D. Gruyter, Structural Characterization of Zeolite Beta, Proceedings of the Royal Society A: Mathematical, Physical and Engineering Sciences. 420 (1988) 375–405. https://doi.org/10.1098/rspa.1988.0131.
[80] M. Gierada, I. Petit, J. Handzlik, F. Tielens, Hydration in silica based mesoporous materials: a DFT model, Physical Chemistry Chemical Physics. 18 (2016) 32962–32972.

[81] M. Gierada, F. De Proft, M. Sulpizi, F. Tielens, Understanding the Acidic Properties of the Amorphous Hydroxylated Silica Surface, J. Phys. Chem. C. 123 (2019) 17343–17352. https://doi.org/10.1021/acs.jpcc.9b04137.
[82] T. Siodla, I. Sobczak, M. Ziolek, F. Tielens, Theoretical and experimental insight into zinc loading on mesoporous silica, Microporous and Mesoporous Materials. 256 (2018) 199–205. https://doi.org/10.1016/j.micromeso.2017.08.008.
[83] J.N. Kondo, E. Yoda, H. Ishikawa, F. Wakabayashi, K. Domen, Acid property of silanol groups on zeolites assessed by reaction probe IR study, Journal of Catalysis. 191 (2000) 275–281.
[84] A. Zecchina, S. Bordiga, G. Spoto, L. Marchese, G. Petrini, G. Leofanti, M. Padovan, Silicalite characterization. 2. IR spectroscopy of the interaction of carbon monoxide with internal and external hydroxyl groups, The Journal of Physical Chemistry. 96 (1992) 4991–4997.

TOC